



# Reduction of Cr(VI) in simulated groundwater by FeS-coated iron magnetic nanoparticles



Yanyan Gong<sup>a</sup>, Longshuang Gai<sup>b</sup>, Jingchun Tang<sup>b,\*</sup>, Jie Fu<sup>c</sup>, Qilin Wang<sup>d</sup>, Eddy Y. Zeng<sup>a</sup>

<sup>a</sup> School of Environment, Guangzhou Key Laboratory of Environmental Exposure and Health, Guangdong Key Laboratory of Environmental Pollution and Health, Jinan University, Guangzhou 510632, China

<sup>b</sup> College of Environmental Science and Engineering, Key Laboratory of Pollution Processes and Environmental Criteria (Ministry of Education), Tianjin Engineering Center of Environmental Diagnosis and Contamination Remediation, Nankai University, Tianjin 300350, China

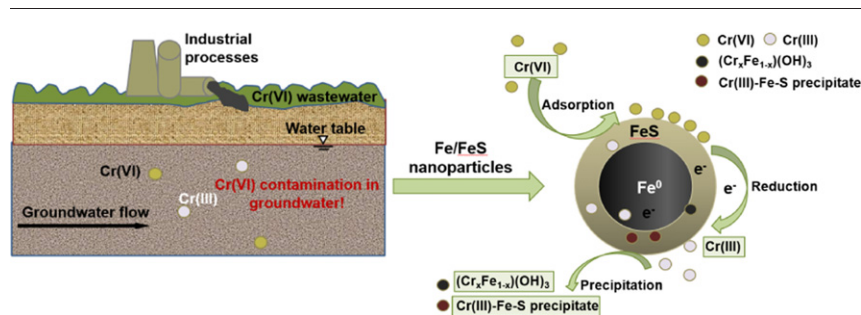
<sup>c</sup> Department of Environmental Science and Engineering, Fudan University, Shanghai 200433, China

<sup>d</sup> Advanced Water Management Centre, The University of Queensland, St Lucia, Queensland 4072, Australia

## HIGHLIGHTS

- FeS coated on Fe<sup>0</sup> surface, effectively inhibited Fe<sup>0</sup> aggregation, and formed Fe/FeS
- Increasing S/Fe molar ratio from 0.138 to 0.207 enhanced Cr(VI) removal by 63%
- Fe/FeS inhibited the leaching of Fe, reducing the toxicity of the particles
- Fe/FeS removed aqueous Cr(VI) mainly by adsorption, reduction, and precipitation
- Fe/FeS effectively removed Cr(VI) through batch and column tests

## GRAPHICAL ABSTRACT



## ARTICLE INFO

### Article history:

Received 23 February 2017

Received in revised form 25 March 2017

Accepted 30 March 2017

Available online 11 April 2017

Editor: Jay Gan

### Keywords:

Fe/FeS nanoparticles

Cr(VI) removal

Groundwater

Remediation

## ABSTRACT

FeS-coated iron (Fe/FeS) magnetic nanoparticles were easily prepared, characterized, and applied for Cr(VI) removal in simulated groundwater. TEM, XRD, and BET characterization tests showed that FeS coating on the surface of Fe<sup>0</sup> inhibited the aggregation of Fe<sup>0</sup> and that Fe/FeS at a S/Fe molar ratio of 0.207 possessed a large surface area of 62.1 m<sup>2</sup>/g. Increasing the S/Fe molar ratio from 0 to 0.138 decreased Cr(VI) removal by 42.8%, and a further increase to 0.207 enhanced Cr(VI) removal by 63% within 72 h. Moreover, Fe/FeS inhibited the leaching of Fe, reducing the toxicity of the particles. Mechanistic analysis indicated that Fe<sup>0</sup>, Fe<sup>2+</sup>, and S<sup>2-</sup> were synergistically involved in the reduction of Cr(VI) to nontoxic Cr(III), which further precipitated as (Cr<sub>x</sub>Fe<sub>1-x</sub>)(OH)<sub>3</sub> and Cr(III)-Fe-S. The process of Cr(VI) sorption by Fe/FeS (S/Fe = 0.207) was fitted well with a pseudo-second-order kinetic model, and the isotherm data were simulated by Langmuir isotherm model with a maximum sorption capacity of 69.7 mg/g compared to 48.9 mg/g for Fe<sup>0</sup>. Low pH and initial Cr(VI) concentration favored Cr(VI) removal. Continuous fixed bed column studies showed that simulated permeable reactive barriers (PRB) with Fe/FeS was considerably effective for in situ removal of Cr(VI) from groundwater. This study demonstrated the high potential of Fe/FeS for Cr(VI) immobilization in water, groundwater, and soil.

© 2017 Elsevier B.V. All rights reserved.

## 1. Introduction

Chromium (Cr) is widely used in industrial processes, including metal electroplating, metal finishing, steelworks manufacturing, leather

\* Corresponding author.

E-mail address: [tangjch@nankai.edu.cn](mailto:tangjch@nankai.edu.cn) (J. Tang).

tanning, and synthesis of pigments (Sarin et al., 2006; Yoon et al., 2011). It is one of the most toxic metals detected in groundwater, surface water, and soils. Cr exists in the environment primarily in two valence states: Cr(III) and Cr(VI) (Li et al., 2012). Cr(VI) species, such as  $\text{HCrO}_4^-$  and  $\text{Cr}_2\text{O}_7^{2-}$ , are soluble in water and exert toxic effects on biological systems due to their strong oxidizing ability (Vainshtein et al., 2003). In contrast, Cr(III) is less hazardous and generally forms highly insoluble minerals. In fact it is an essential microelement for organisms at low concentrations (Sarkar et al., 2010; Villacis-Garcia et al., 2015). Techniques such as adsorption (Sarkar et al., 2010; Wang et al., 2015a), photocatalytic reduction (Wang et al., 2015b; Wang et al., 2015c), and membrane separation (Çengelöglu et al., 2003) have been applied for Cr(VI) removal. However, these technologies exist some deficiencies, such as costly and production of other waste problems. Reduction of Cr(VI) to relatively nontoxic Cr(III) followed by chemical precipitation is a common method to mitigate Cr(VI) (Gupta et al., 2011; Lee et al., 2013; Wilkin et al., 2005).

Various reducing materials such as zero valent iron (ZVI) (Melitas et al., 2001; Shi et al., 2011), divalent iron (Fe(II)) (Schlautman and Han, 2001), and iron sulfide (Kantar et al., 2015; Patterson and Fendorf, 1997) have been investigated for the reduction of Cr(VI) to Cr(III). ZVI is regarded as one of the most effective reductants due to its strong reactivity, low cost, and easy separation and disposal (Crane and Scott, 2012; Fu et al., 2014). However, there are still challenges with environmental application, such as high toxicity and aggregation of ZVI particles (Keller et al., 2012; Li et al., 2016). Moreover, ZVI is not thermodynamically stable in water and is subject to corrosion by water itself, producing gases such as hydrogen or dinitrogen (Gong et al., 2016).

Iron sulfide (FeS), a tetragonal ferrous monosulfide, has been widely applied for treatment of heavy metals, including  $\text{Cd}^{2+}$ ,  $\text{Zn}^{2+}$ ,  $\text{Hg}^{2+}$ ,  $\text{Cu}^{2+}$ , and  $\text{Mn}^{2+}$  due to its unique surface chemical properties and molecular structure (Wharton et al., 2000). Typically, the metals are removed through sorption, ion exchange, and/or precipitation of highly insoluble metal sulfides (Gong et al., 2016). FeS is an important reductant providing a source of Fe(II) and S(-II) species, which can act as electron donors and facilitate Cr(VI) reduction (Demoisson et al., 2005; Mullet et al., 2004).

Combining iron sulfide with ZVI (Fe/FeS) may be a feasible method for preparing multicomponent nanoparticles, which can possess unique physical and chemical properties due to a synergistic effect induced by interaction between individual components. For instance, incorporation of FeS to ZVI can slow down the releasing rate of  $\text{Fe}^{2+}$  from the core ZVI (Saleh et al., 2008; Xiu et al., 2010), reducing the toxicity of ZVI; the presence of FeS can prevent the aggregation of ZVI (Li et al., 2016; Li et al., 2012) and greatly decrease the chance of Cr(III) reoxidation (Lan et al., 2005; Patterson and Fendorf, 1997). Recently, Kim et al. (2011) developed a simple synthesis process to prepare Fe/FeS particles and the particles were successfully applied for faster and more efficient removal of trichloroethylene (TCE) from water than pure  $\text{Fe}^0$  nanoparticles. Su et al. (2015) reported that FeS/Fe at an S/Fe molar ratio of 0.28 had the maximum sorption capacity of 85 mg/g for  $\text{Cd}^{2+}$ , which was > 100% higher than that for pure ZVI. Aging the particles for three weeks had no negative effect on  $\text{Cd}^{2+}$  removal and Cd-containing mixture remained stable for two months. Compared to ZVI particles, the Fe/FeS nanoparticles exhibit some advantages such as larger surface area, higher reactivity, stronger magnetic responsivity, longer reactive longevity, and possibly greater affinity towards many heavy metals, and thus, the nanoparticles have the potential to be used as ideal reactive materials for environmental remediation.

The overall goal of the present study was to investigate the removal efficiency and mechanisms of aqueous Cr(VI) via Fe/FeS magnetic nanoparticles. The nanoparticles were synthesized using simple one-pot method. The specific objectives were to (1) evaluate the influence of different S/Fe molar ratios on the physicochemical characteristics and Cr(VI) removal efficiency of Fe/FeS; (2) examine the effects of pH and

initial Cr(VI) concentrations on the Cr(VI) removal by Fe/FeS; (3) explore the underlying removal mechanisms; and (4) test the performance of Fe/FeS acting as a reactive material in permeable reactive barriers (PRB) for Cr(VI) removal in groundwater through column tests.

## 2. Materials and methods

### 2.1. Chemicals

All chemicals used in this study were of analytical grade or better. Ferric chloride ( $\text{FeCl}_3 \cdot 6\text{H}_2\text{O}$ , 99%, analytical grade), sodium dithionite ( $\text{Na}_2\text{S}_2\text{O}_4$ , 95%, analytical grade), sodium borohydride ( $\text{NaBH}_4$ , 98%, analytical grade), NaOH (analytical grade), and HCl (analytical grade) were provided by Jiangtian Chemical (Tianjin, China). Potassium dichromate ( $\text{K}_2\text{Cr}_2\text{O}_7$ , 99.5%, guaranteed grade) was purchased from Guangfu Technology Development (Tianjin, China). All solutions were prepared with  $\text{N}_2$ -purged deionized (DI) water.

### 2.2. Preparation and characterization of Fe/FeS particles

Fe/FeS particles were prepared following a revised version of the approach by Kim et al. (2011). Briefly,  $\text{FeCl}_3 \cdot 6\text{H}_2\text{O}$  (14.48 g) was dissolved in 900 mL of DI water, and an 100-mL solution containing 9.74 g  $\text{NaBH}_4$  with various amounts of dithionite (0, 0.32, 0.64, and 0.96 g, respectively) (pH 10.1) was added dropwise to the  $\text{FeCl}_3$  solution (pH 1.9). Particles with S/Fe molar ratios of 0 (or  $\text{Fe}^0$ ), 0.070, 0.138, and 0.207 were obtained. Preliminary tests showed that particles were no longer magnetic at an S/Fe molar ratio > 0.207, therefore, particles with S/Fe molar ratios  $\leq 0.207$  were chosen for further investigations. The mixture (pH 9.0) was idle for 15 min after reduction. The resultant particles were collected using a permanent magnet, rinsed with DI water three times, and subsequently freeze-dried in a vacuum freeze dryer (FD5-3, SIM International Group, CA, USA). All the particles were sealed under  $\text{N}_2$  protection prior to use.

Surface morphology was obtained by a T-20 transmission electron microscope (TEM, JEM-2100, JEOL, Japan). Specific surface area was examined with a BET adsorption method (ASAP2460, Micromeritics, Atlanta, GA, USA). Zeta potential was measured with a Zetasizer Nano ZS90 (Malvern Instruments, Malvern, UK). The crystalline compositions were investigated by X-ray diffractometer (XRD) (D/max-2500, Rigaku, Tokyo, Japan). X-ray photoelectron spectroscopy (XPS, PHI-5000, Ulvac-Phi, Japan) was used to determine the surface elemental compositions of the particles and XPS spectra were analyzed using CasaXPS software (version 2.3.18). Gaussian (Y%)–Lorentzian (X%) was defined in CasaXPS as GL(X) (Fairley, 2016) and the elements peaks (S2p, Fe2p, and Cr2p) fitted best with a GL (30) line shape in this study. The magnetic properties of the particles were measured with a magnetic measuring system (Squid-vsm, Quantum Design, USA).

### 2.3. Effects of S/Fe molar ratios on Cr(VI) removal by Fe/FeS

Batch experiments were performed in sealed 40-mL glass vials under anoxic conditions. Fe/FeS particles with different S/Fe molar ratios (0, 0.070, 0.138, and 0.207) (0.012 g) were added to the vials, followed by the addition of 40-mL 25 mg/L Cr(VI) solutions. pH of the mixture was maintained at  $5.0 \pm 0.3$  with HCl (0.1 M) and NaOH (0.1 M). The vials were then mixed at 40 rpm on an end-over-end rotator at  $25 \pm 1$  °C. At predetermined time intervals, duplicate vials were sacrificially sampled. Magnet was used to separate the particles from the solution within 5 min and 10 mL supernatant was collected for Cr(VI), total Cr (TCr), and Fe analysis. Control tests without the addition of the particles were performed to evaluate the loss of Cr(VI) under otherwise identical conditions. All the experiments were conducted in duplicate.

#### 2.4. Effects of pH and initial Cr(VI) concentrations on Cr(VI) removal by Fe/FeS

To investigate the pH effect, batch tests were carried out in sealed 40-mL glass vials with 0.3 g/L Fe/FeS particles (S/Fe molar ratio = 0.207) and 25 mg/L Cr(VI) at constant pH of 3.5, 5.0, 7.1, and 9.0, respectively. To explore the initial Cr(VI) concentration effect, Cr(VI) removal tests were carried out at various Cr(VI) concentrations of 10, 15, 25, 35, 50, and 80 mg/L with a fixed pH of  $5.0 \pm 0.3$  and the dosage of Fe/FeS (S/Fe = 0.207) or Fe<sup>0</sup> were 0.3 g/L.

#### 2.5. Fixed-bed column experiments

To assess the effectiveness of Cr(VI) removal by Fe/FeS under dynamic flow conditions similar to those observed in situ PRB, column experiments were performed in a glass column with a height of 12 cm and an internal diameter of 10 mm (Omnifit, Cambridge, England). The column was wet-packed with 0.12 g of Fe/FeS (height = 0.30 cm) between two layers of 50–70 mesh quartz sands (height of each layer = 5.85 cm) (Fig. 1). The sands were pretreated prior to use following a reported method (Johnson et al., 1996). The influent solution of 25 mg/L Cr(VI) (initial pH = 5.0) was pumped into the column in a down flow mode using a PHD/ULTRA infusion syringe pump (Harvard Apparatus, Holliston, MA, USA) at a flow rate of 0.2 mL/min. All the solutions were purged with N<sub>2</sub>. A control column packed with quartz sand (height = 12 cm) was tested under the same conditions. Samples of the effluent were collected periodically for measurements of Cr(VI) and pH.

#### 2.6. Chemical analysis

pH value was determined with a pH meter (PB-10, Sartorius, Goettingen, Germany). Concentrations of aqueous Cr(VI) were determined with the diphenylcarbazide method (Altundogan, 2005) using UV-visible spectrophotometer (UV-754, Tianjin, China) at a wavelength of 540 nm and the detection limit was 0.004 mg/L. Total Fe and TCr concentrations were measured by ICP-AES (IRIS Intrepid II XSP, Thermo Scientific, Waltham, MA, USA) and the detection limits were 4.0 µg/L for TCr and 2.0 µg/L for total Fe.

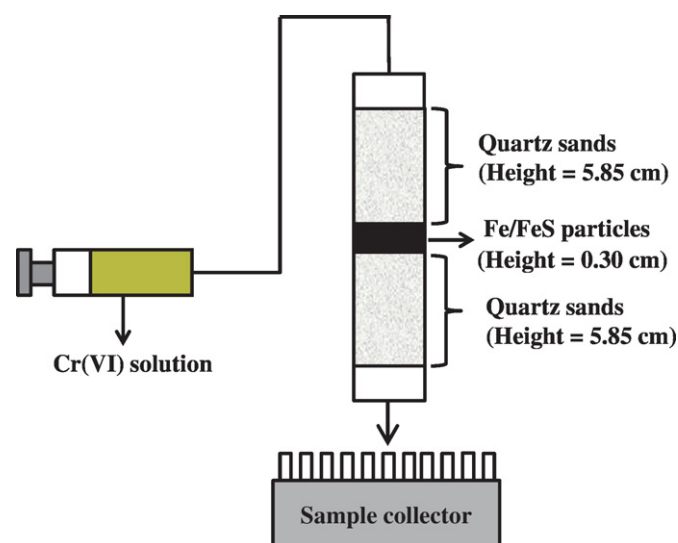


Fig. 1. Fixed-bed column setup.

### 3. Results and discussion

#### 3.1. Characterization of Fe/FeS and reaction mechanisms of Cr(VI) removal by Fe/FeS

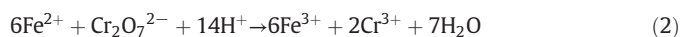
TEM images of Fe<sup>0</sup> and Fe/FeS (S/Fe = 0.207) particles (Fig. S1) demonstrated that the FeS coating effectively prevented Fe<sup>0</sup> from aggregating. The occurrence of Fe<sup>0</sup> in agglomerates was probably caused by magnetic dipole interactions and chemical aggregation (Martin et al., 2008). Fe/FeS particles composed of a core of Fe<sup>0</sup> (a diameter of 70 nm) covered with an amorphous FeS shell (Su et al., 2015), akin to a spherical core-shell structure. BET surface areas of Fe/FeS particles with various S/Fe molar ratios (0 (Fe<sup>0</sup>), 0.070, 0.138, and 0.207) was measured to be 8.9, 5.4, 4.9, and 62.1 m<sup>2</sup>/g, respectively. Fe/FeS with a S/Fe molar ratio of 0.207 presented the largest BET surface area, six times higher than Fe<sup>0</sup>. Various extent of sulfidation may cause different surface morphologies and impart particles with different surface functional groups. Introduction of FeS to the iron can increase the surface roughness of particles (Kim et al., 2011), and thus affecting the surface area. Fe/FeS (S/Fe = 0.207) exerting the largest BET surface area was probably due to the higher S content.

Zeta potentials of Fe/FeS with different S/Fe ratios were variable in the pH range of 3–9 (Fig. S2). It should be noted that Fe<sup>0</sup> and Fe/FeS (S/Fe = 0.07, 0.138, and 0.207) were positively charged under acidic conditions (pH = 3–7) and negatively charged at pH range from 7 to 9, resulting in an isoelectric point (IEP) of 7.1 for all particles. The IEP of Fe<sup>0</sup> was similar to previously reported values (IEP value at 7.0–8.0) (Giasuddin et al., 2007). It is reported that the IEP of pristine FeS was 7.5 (Wolthers et al., 2005). The IEP of Fe/FeS particles did not change with the variation of S/Fe molar ratios owing to the low contents of FeS covered on the Fe<sup>0</sup> surface. The positively charged surface of Fe/FeS at acidic pH may contribute to Cr(VI) removal via electrostatic interaction.

The magnetic properties of Fe<sup>0</sup> and Fe/FeS (S/Fe = 0.207) particles were measured by a vibrating sample magnetometer at room temperature, and the results were shown in Fig. 2a and b. The saturation magnetization (M<sub>s</sub>) of Fe<sup>0</sup> was 165.6 emu/g and the M<sub>s</sub> value decreased to 78.0 emu/g when FeS was coated to the iron. The different M<sub>s</sub> values of these two samples can be explained by the different compositions, which were attributed to the S content on the particles (Wang et al., 2017). As seen in the insets of Fig. 2, when a permanent magnet is applied, Fe<sup>0</sup> and Fe/FeS particles were completely separated after 2 min and 5 min, respectively, demonstrating easy separation performance.

XRD diffractograms of Fe<sup>0</sup> and Fe/FeS particles were compared (Fig. 3a). For Fe<sup>0</sup>, the characteristic diffraction peak at 44.7° corresponded to the body-centered cubic Fe<sup>0</sup> with a relatively poor crystallinity (Zhang et al., 2013). The peak for Fe/FeS particles at the same 2θ value was strengthened. Typical peaks at 2θ = 44.7°, 34.9°, and 64.5° were assigned to the phases (211), (102), (220) for iron sulfide (FeS), respectively (PDF# 89-6268). However, the characteristic peaks of FeS at 34.9° and 64.5° were weak probably due to the low concentration or low degree of crystallinity. The diffraction peaks of S<sup>0</sup> was not discerned in the XRD analysis. The XRD results indicated that Fe/FeS was a hybrid material with the coexistence of Fe<sup>0</sup> and FeS.

To probe the interactions between Cr(VI) and Fe/FeS, XRD were also performed after Cr(VI) uptake (Fig. 3b). Upon Cr(VI) reaction with Fe<sup>0</sup>, one distinct new diffraction at 21.8° indicated the formation of sparingly soluble Cr(III)-Fe(III) mixed hydroxide (PDF# 30-0648) as shown in Eqs. (1)–(3) (Manning et al., 2007):



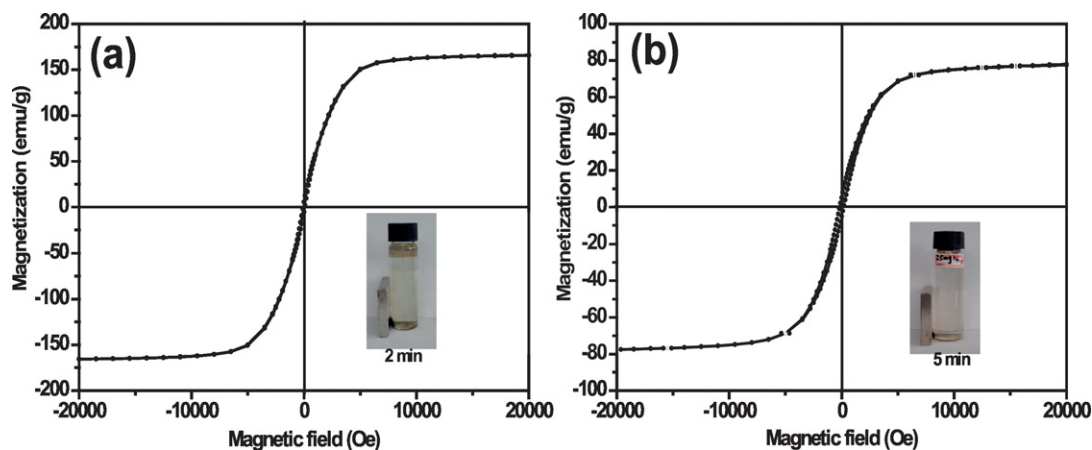
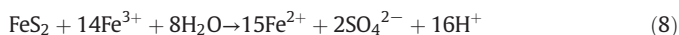
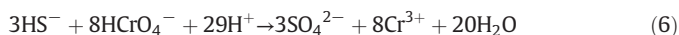
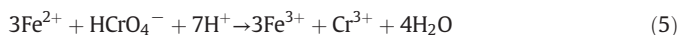


Fig. 2. Magnetization curves of (a)  $\text{Fe}^0$  and (b)  $\text{Fe}/\text{FeS}$  ( $\text{S}/\text{Fe} = 0.207$ ) nanoparticles. Inset: (a) digital photographs of  $\text{Fe}^0$  particles in response to a permanent magnet after 2 mins; and (b) the response of  $\text{Fe}/\text{FeS}$  to a magnet after 5 mins.



Upon reaction of  $\text{Cr}(\text{VI})$  with  $\text{Fe}/\text{FeS}$ , the diffraction peaks at  $2\theta$  of  $35.8^\circ$ ,  $44.5^\circ$ ,  $58.3^\circ$ , and  $64.7^\circ$  corresponded to the characteristic peaks of daubreelite ( $\text{FeCr}_2\text{S}_4$ , PDF# 04-0651).

The electronic structures and chemical compositions of  $\text{Fe}/\text{FeS}$  before and after reaction with  $\text{Cr}(\text{VI})$  at pH 5.0 were characterized by XPS (Fig. 4). The elemental compositions of  $\text{Fe}/\text{FeS}$  particles were Fe (24.1%), S (3.5%), and oxygen (72.4%), and changed to Fe (11.3%), S (4.4%), oxygen (73.4%), and Cr (10.9%) after reaction. For  $\text{Fe}/\text{FeS}$  particles, the binding energies of  $\text{S}2\text{p}$  at 161.3, 162.8, and 168.1 eV correspond to  $\text{FeS}$  (Pratt et al., 1994; Stypula and Stoch, 1994),  $\text{FeS}_2$  (Donato et al., 1993), and surface bound  $\text{SO}_4^{2-}$  (Thomas et al., 1998), respectively. After reaction with  $\text{Cr}(\text{VI})$ ,  $\text{FeS}$  decreased from 54.9% to 10.8% (shifted from 161.3 to 160.2 eV), and  $\text{FeS}_2$  at 162.8 eV was oxidized to  $\text{Fe}-\text{S}_n^{2-}$  at 162.9 eV (Nesbitt and Muir, 1994). The formation of  $\text{Fe}-\text{S}_n^{2-}$  resulted from the oxidation of  $\text{FeS}$  and  $\text{FeS}_2$  associated with  $\text{Cr}(\text{VI})$  reduction (Nesbitt and Muir, 1994). Moreover,  $\text{SO}_4^{2-}$  increased from 28.8% to 40.1% (shifted from 168.1 to 167.7 eV) (Neal et al., 2001). This indicated that  $\text{FeS}$  or  $\text{FeS}_2$  reacted with  $\text{Cr}(\text{VI})$  resulting in the oxidation of sulfur (Eqs. (4)–(8)) (Demoisson et al., 2005; Mullet et al., 2004).



For  $\text{Fe}/\text{FeS}$  particles, binding energies of  $\text{Fe}2\text{p}$  centered at 710.8 eV was assigned to  $\text{Fe}(\text{III})-\text{S}$  (Nesbitt and Muir, 1994), and the peak at 712.6 eV and 724.2 eV were attributed to  $\text{FeOOH}$  compounds (Biesinger et al., 2011; Pratt et al., 1994; Tang et al., 2016). These species may be ascribed to the oxidation of  $\text{Fe}^0$  or  $\text{Fe}^{2+}$  by  $\text{O}_2$  in air (Mullet et al., 2008). The binding energies of  $\text{Fe}2\text{p}$  at 709.5 eV was ascribed to  $\text{Fe}^{2+}$  and the peak located at 715.7 eV was a broad  $\text{Fe}^{2+}$  satellite (Castro and Ciampi, 1995; Yamashita and Hayes, 2008). There was no obvious peak corresponding to  $\text{Fe}^0$  owing to the coating of  $\text{FeS}$  on the surface of  $\text{Fe}^0$ . After  $\text{Cr}(\text{VI})$  uptake,  $\text{Fe}^{2+}$  decreased from 23.0% to 22.0% (shifted from 709.5 and 715.7 eV to 709.6 and 718.2 eV). Meanwhile,  $\text{Fe}(\text{III})-\text{S}$  increased from 29.7% to 33.5% (shifted from 710.8 to 710.9 eV) and  $\text{FeOOH}$  decreased from 30.2% to 25.6% (shifted from 712.6 to 712.7 eV). The increase in  $\text{Fe}(\text{III})-\text{S}$  may result from the breakage of  $\text{Fe}-\text{S}$  bonds by transferring an electron from  $\text{Fe}$  to  $\text{Cr}(\text{VI})$ , thus leading to the formation of  $\text{Fe}(\text{III})$  at the surface. The binding energy of  $\text{Cr}2\text{p}$

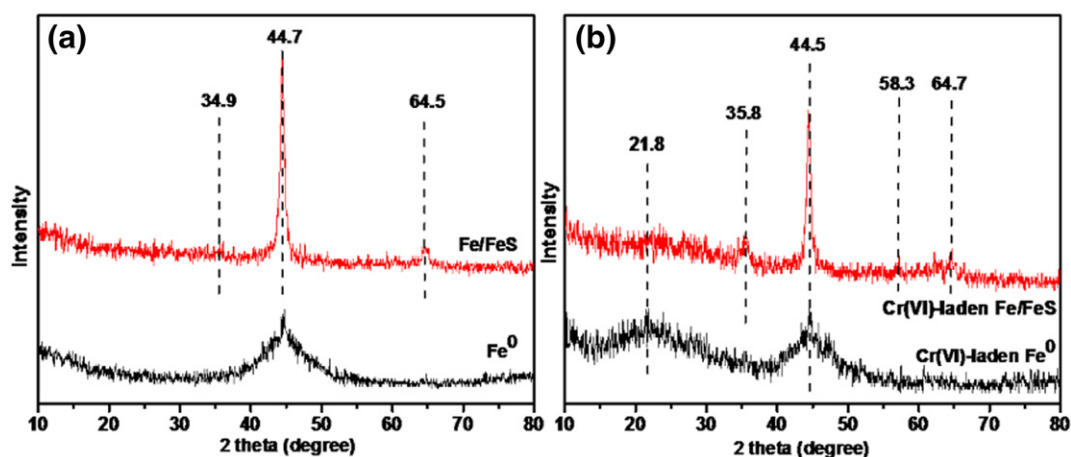


Fig. 3. XRD spectra of (a)  $\text{Fe}^0$  and  $\text{Fe}/\text{FeS}$  ( $\text{S}/\text{Fe} = 0.207$ ) and (b)  $\text{Cr}(\text{VI})$ -laden  $\text{Fe}^0$  and  $\text{Cr}(\text{VI})$ -laden  $\text{Fe}/\text{FeS}$  ( $\text{S}/\text{Fe} = 0.207$ ) particles. The  $\text{Cr}(\text{VI})$ -laden particles were prepared by equilibrating the respective particles (0.3 g/L) with 25 mg/L  $\text{Cr}(\text{VI})$  at pH 5.0.

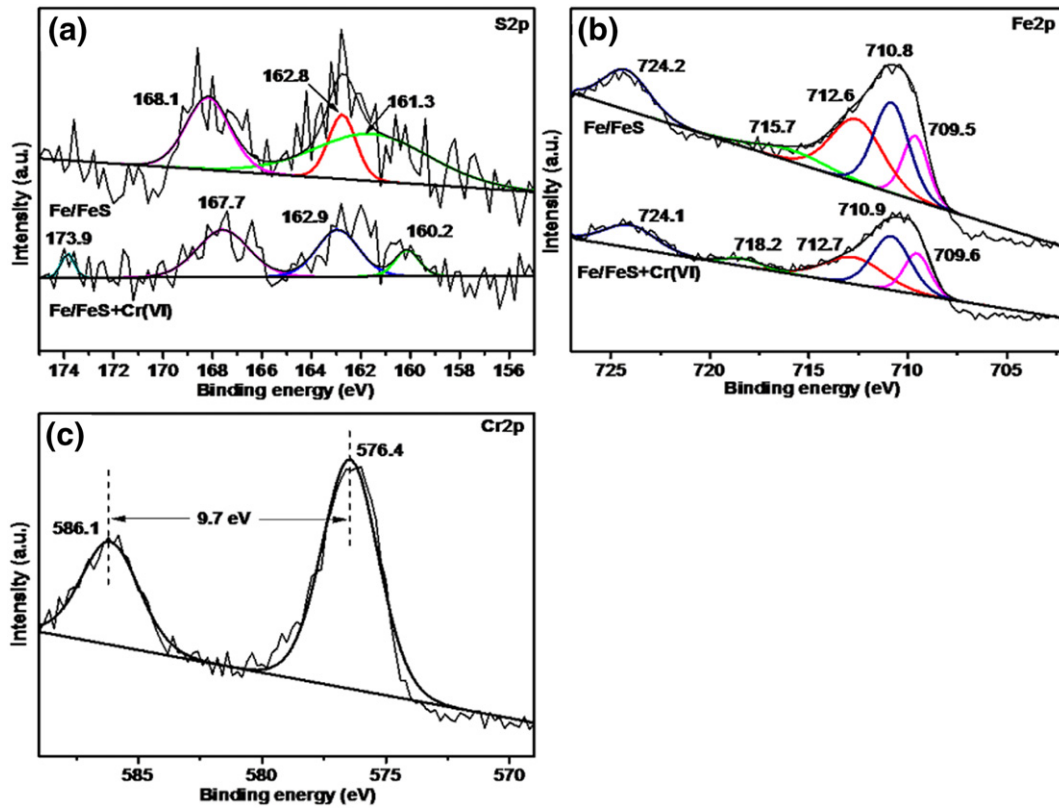


Fig. 4. XPS spectra of Fe/FeS and Cr-laden Fe/FeS (S/Fe = 0.207): (a) S2p, (b) Fe2p, (c) Cr2p. Initial Cr(VI) = 25 mg/L, Fe/FeS = 0.3 g/L, constant pH = 5.0 ± 0.3, and reaction time = 72 h.

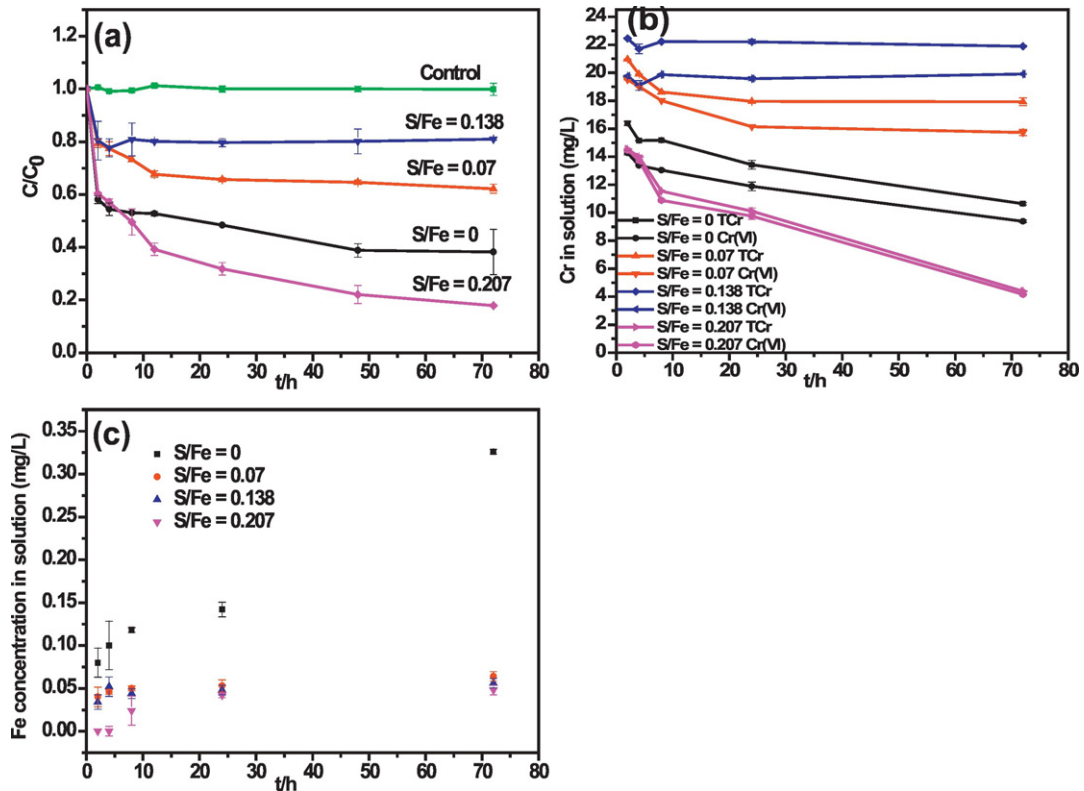


Fig. 5. (a) Effects of S/Fe molar ratios on removal rate of Cr(VI) by Fe/FeS; (b) aqueous TCr and Cr(VI) concentrations upon reaction of Cr(VI) with Fe/FeS particles; and (c) dissolved Fe concentration after Cr(VI) reduction with Fe/FeS particles. Initial Cr(VI) = 25 mg/L, Fe/FeS = 0.3 g/L, constant pH = 5.0 ± 0.3, and temperature = 25 ± 1 °C.

was centered at 576.4 eV and the spin orbit splitting was 9.7 eV (Fig. 4c), which corresponds to Cr(III) (Mullet et al., 2007), confirming the transformation of Cr(VI) to Cr(III) in the form of  $(Cr_xFe_{1-x})(OH)_{3(s)}$  or  $Cr(OH)_3$  as described in Eqs. (1)–(3).

In summary, removal of Cr(VI) by Fe/FeS magnetic nanoparticles mainly involved the following processes: (a) adsorption of Cr(VI) anions by electrostatic attraction to the Fe/FeS surface in acid solution; (b) oxidation–reduction between  $Fe^0$ , FeS,  $FeS_2$ , and Cr(VI), resulting in the formation of  $Fe^{2+}$ ,  $Fe^{3+}$ ,  $SO_4^{2-}$ , and Cr(III); and (c) precipitation of Cr(III) in the form of  $(Cr_xFe_{1-x})(OH)_3$  and  $FeCr_2S_4$ .

### 3.2. Effects of different S/Fe molar ratios on Cr(VI) removal

The efficacy of Cr removal by Fe/FeS particles was strongly affected by the S/Fe molar ratios (Fig. 5a). The normalized residual concentration  $C/C_0$  was used to describe the removal rate. Control experiments showed that Cr(VI) did not adsorb to the vials.  $Fe^0$  (S/Fe = 0) removed 61.8% of 25 mg/L Cr(VI) at pH 5.0 within 72 h. In the presence of Fe/FeS (S/Fe = 0.07, 0.138, and 0.207), the removal rate was 37.8%, 19.0%, and 82.1%, respectively. Similar findings were also reported in the removal of Cd by FeS/Fe (Su et al., 2015). The sequence for Cr(VI) removal efficiency is consistent with the surface area results, illustrating that surface adsorption played an important role during the reaction.

The highest removal efficiency of Fe/FeS (S/Fe = 0.207) can be attributed to the optimal FeS arrangement on the  $Fe^0$  surface. As discussed before, FeS was coated on the surface of  $Fe^0$  as a shell or cover. Cr(VI) as an electron acceptor was reduced to Cr(III) by electrons supplied from  $Fe^0$ , FeS, and  $FeS_2$ . The presence of FeS on the surface of  $Fe^0$  could facilitate the reduction of Cr(VI) via electron acceptance: (1) electrons generated by  $Fe^0$  could be spontaneously transferred to the surface FeS semiconductor due to its higher electronegativity (5.02 eV) (Xu and Schoonen, 2000) than that of  $Fe^0$  (4.04 eV) (Pearson, 1988) and

(2) FeS itself is a strong reductant and has a good electron conductivity with a low band gap ( $E_g = 0.1$  eV).

The aqueous TCr and Cr(VI) concentrations varied over time during the reactions of Cr(VI) with  $Fe^0$  and Fe/FeS particles (Fig. 5b). The difference between the concentrations of TCr and Cr(VI) was aqueous Cr(III) concentration. The decline in Cr(VI) was due to the reduction to Cr(III) by  $Fe^0$  and Fe/FeS particles, and the decrease in TCr was ascribed to the precipitation of Cr(III) on the surface of the particles. It is noteworthy that for Fe/FeS (S/Fe = 0.207), aqueous chromium remaining were in the form of Cr(VI), and no aqueous Cr(III) were detected. The much lower aqueous Cr(III) concentration in the presence of Fe/FeS compared to  $Fe^0$  can be explained by the fact that Cr(III) precipitated in forms of both  $(Cr_xFe_{1-x})(OH)_3$  and  $FeCr_2S_4$  in the presence of FeS.

Total dissolved iron reached 0.33 mg/L after Cr(VI) reduction with  $Fe^0$  within 72 h, while the iron concentration sharply declined for Fe/FeS particles (Fig. 5c). The dissolved Fe concentration decreased from 0.33 to 0.048 mg/L with an increase of the S/Fe ratio from 0 to 0.207. The presence of FeS can block the active sites on the  $Fe^0$  surface thereby retarding the dissolution of iron core (Kim et al., 2011). Also, the formation of  $(Cr_xFe_{1-x})(OH)_3$  and Cr(III)-Fe-S precipitation consumed iron, reducing the total Fe in the solution. On the other hand, the decrease of total dissolved Fe concentration after reduction demonstrated that Fe/FeS would pose lower toxicity risks compared to  $Fe^0$ , whose toxicity was partly due to Fe(II) and Fe(III) ions in solution (Keller et al., 2012). Therefore, the Fe/FeS particles prepared with a simple procedure showed higher Cr(VI) removal efficiency and better biocompatibility than  $Fe^0$ .

### 3.3. Effects of pH on Cr(VI) removal

Removal of Cr(VI) by Fe/FeS was strongly pH-dependent. The removal efficiency decreased from 88.8% to 34.2% as pH increased from 3.5 to 9.0 within 72 h (Fig. 6a). The commonly used pseudo-first-order

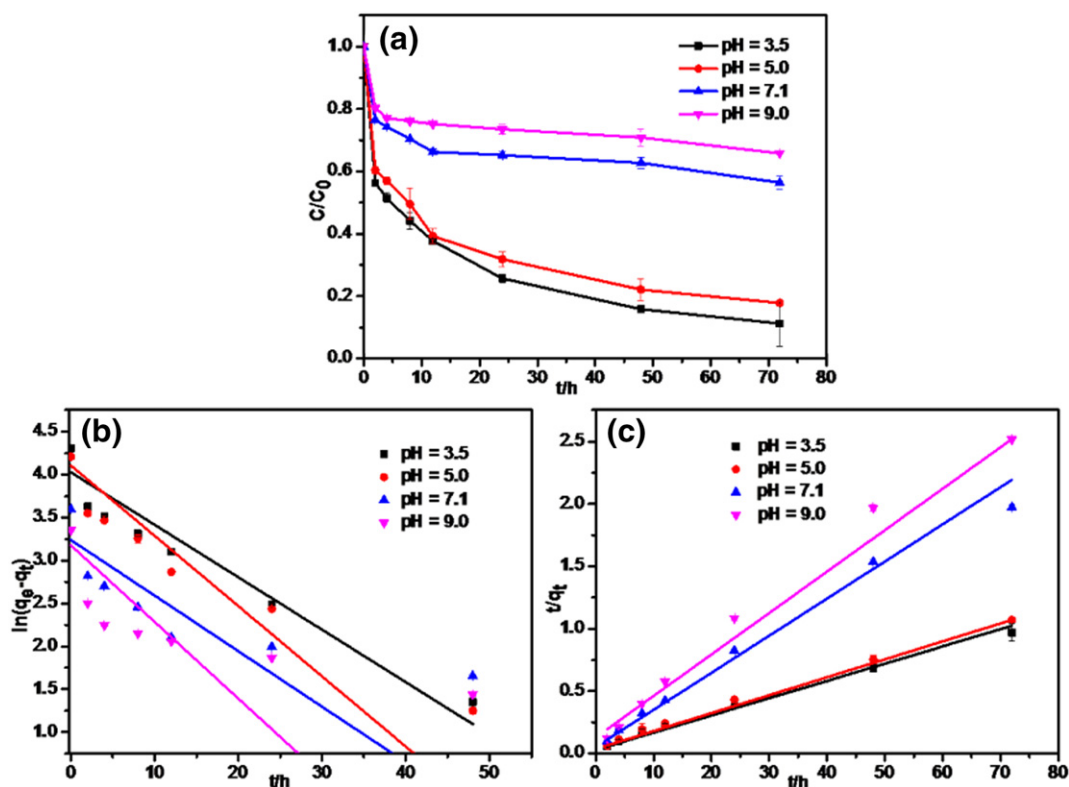
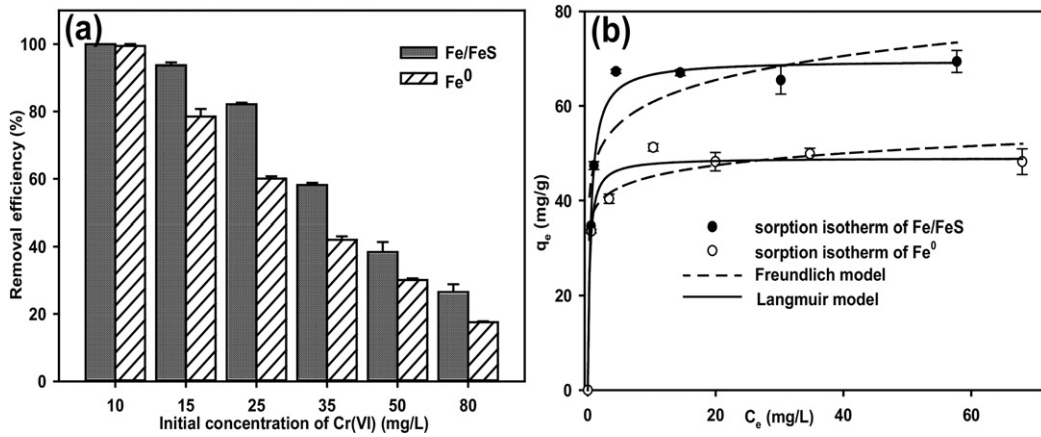


Fig. 6. (a) Effects of pH on removal of Cr(VI) by Fe/FeS (S/Fe = 0.207), (b) pseudo-first-order kinetic model, and (c) pseudo-second-order kinetic model for removal of Cr(VI) by Fe/FeS at various pH values. Fe/FeS = 0.3 g/L, initial Cr(VI) = 25 mg/L, and temperature = 25 ± 1 °C.



**Fig. 7.** (a) Effects of initial Cr(VI) concentrations on removal efficiency of Cr(VI) by Fe/FeS ( $S/Fe = 0.207$ ) and  $Fe^0$  particles; (b) Cr(VI) sorption isotherm of Fe/FeS ( $S/Fe = 0.207$ ) and  $Fe^0$  (Symbols: experimental data; lines: model fittings).  $Fe/FeS$  or  $Fe^0 = 0.3$  g/L, constant  $pH = 5.0 \pm 0.3$ , and temperature =  $25 \pm 1$  °C.

and pseudo-second-order models were applied to simulate the kinetic data at different pH values (Fig. 6b and c) (Gong et al., 2014):

$$\ln(q_e - q_t) = \ln q_e - K_1 t \quad \text{Pseudo-first-order model} \quad (9)$$

$$\frac{t}{q_t} = \frac{1}{K_2 q_e^2} + \frac{t}{q_e} \quad \text{Pseudo-second-order model} \quad (10)$$

where  $q_e$  and  $q_t$  (mg/g) are the amounts of Cr(VI) removed at equilibrium and at different time  $t$  (h), respectively; and  $K_1$  (1/h) and  $K_2$  (g/(mg·h)) are the sorption rate constants of pseudo-first-order and pseudo-second-order models, respectively. Apparently, the pseudo-second-order model provided better fitting than the pseudo-first-order model (Table S1), which was consistent with the findings by Yang et al. (2014), who modeled the Cr(VI) sorption kinetics by C/FeS/Fe. The results illustrated that the removal of Cr(VI) was predominantly chemisorption process (Inyang et al., 2014).

pH can inhibit Cr(VI) removal in several ways. First, the IEP of Fe/FeS ( $S/Fe = 0.207$ ) was 7.1, and Fe/FeS was negatively charged in an alkaline solution, hindering the adsorption of Cr(VI) due to electrostatic repulsion. Second, the acidic condition favored the dissolution of FeS releasing  $Fe^{2+}$  and  $S^{2-}$ . Moreover, the free and surface bound ferrous ions were more easily oxidized at higher pH, forming thick hydroxide layers on the surface and inhibiting  $Fe^0$  corrosion (Powell et al., 1995).

#### 3.4. Effects of initial Cr(VI) concentrations on Cr(VI) removal

An increase of initial Cr(VI) concentration from 10 to 80 mg/L decreased the Cr(VI) removal efficiency from 99.9% to 26.5% by 0.3 g/L Fe/FeS and from 99.4% to 17.5% by  $Fe^0$  within 72 h (Fig. 7a). For a fixed dosage of Fe/FeS, the total available active sites are limited. The higher removal efficiency of Fe/FeS at low initial Cr(VI) concentration could be attributed to the high ratio of initial molar numbers of Cr(VI) to the available active sites on the surface (Fu et al., 2015). An increased Cr(VI) concentration approaching Fe/FeS could promote the formation of Cr(III)-Fe-S or  $(Cr_xFe_{1-x})(OH)_3$  precipitates on the Fe/FeS surface, accelerating Fe/FeS passivation. The passivated layer would further limit Cr(VI) diffusion, reduce the electron transfer from the Fe/FeS to Cr(VI), and accordingly retard the reduction of Cr(VI) (Alidokht et al., 2011).

Langmuir and Freundlich isotherm models were applied to describe the Cr(VI) sorption process by Fe/FeS and  $Fe^0$  (Fig. 7b and Table S2). The Langmuir model ( $R^2 = 0.992$  for Fe/FeS and 0.980 for  $Fe^0$ ) outperformed the Freundlich model ( $R^2 = 0.933$  for Fe/FeS and 0.969 for  $Fe^0$ ), indicating a monolayer sorption process of Cr(VI) on the surface of Fe/FeS and  $Fe^0$  particles. The Langmuir maximum sorption capacity of Cr(VI) was 69.7 mg/g for Fe/FeS, which was 42.5% higher than that of  $Fe^0$  (48.9 mg/g). Moreover, the maximum sorption capacity was much

higher than some reported iron-based materials (Alidokht et al., 2011; Ponder et al., 2000; Shi et al., 2011). For instance, Alidokht et al. (2011) reported a maximum Cr(VI) sorption capacity of 33.3 mg/g for starch-stabilized  $Fe^0$  nanoparticles at pH 5.

#### 3.5. Column tests

Column experiments were carried out to determine the removal efficacy of Cr(VI) by  $Fe^0$  and Fe/FeS particles in continuous flows. The temporal changes in the concentrations of dissolved Cr(VI) through a column packed with pure quartz sands (control tests) or quartz sands with Fe/FeS or  $Fe^0$  were compared (Fig. 8). For the control tests, Cr(VI) concentration in the effluent sharply increased from 0 to 25 mg/L (i.e.,  $C/C_0 = 1$ ) after two pore volumes (PVs), reaching complete breakthrough. The Cr(VI) concentration gradually increased from 0 to 3.94 mg/L ( $C/C_0 = 0.16$ ) after 12 PVs for Fe/FeS column and to 2.45 mg/L ( $C/C_0 = 0.10$ ) after 20 PVs for  $Fe^0$  column. Full breakthrough of Cr(VI) occurred at 146 PVs for Fe/FeS, compared to 105 PVs for  $Fe^0$ . At full breakthrough, 70% of the influent Cr(VI) exited the column and remained constant ( $C/C_0 = 0.7$ ) for Fe/FeS, indicating that 30% Cr(VI) was removed continuously, while the breakthrough curve of Cr(VI) reached a plateau at  $C/C_0 = 0.85$  (15% removal at steady state) for  $Fe^0$ .

For both Fe/FeS and  $Fe^0$  packed columns, pH values of the effluents increased initially and then decreased. For example, for Fe/FeS, pH

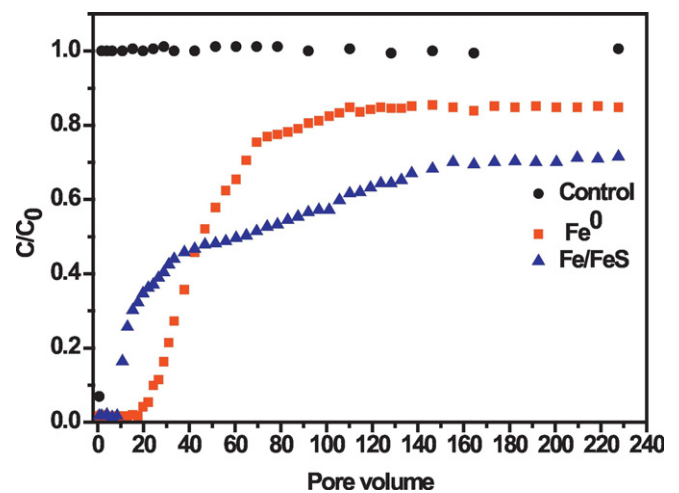


**Fig. 8.** Breakthrough curves of Cr(VI) through a column packed with pure quartz sands (control) or quartz sands with  $Fe^0$  or Fe/FeS ( $S/Fe = 0.207$ ). Initial Cr(VI) = 25 mg/L, Fe/FeS particles = 0.12 g, initial pH = 5.0, flow rate = 0.2 mL/min, and temperature =  $25 \pm 1$  °C.

increased from initial 5.0 to 6.7 after 100 PVs and then decreased to 5.4 after 230 PVs. The pH change was consistent with the abovementioned Cr(VI) removal mechanisms. The oxidation of  $\text{Fe}^0$ ,  $\text{Fe}^{2+}$ , and  $\text{S}^{2-}$  produced  $\text{OH}^-$  or consumed  $\text{H}^+$  in the solution, leading to an increase in pH (Eqs. (1)–(2) and (4)–(7)) (Alowitz and Scherer, 2002), and then, the precipitation of Cr(III) consumed  $\text{OH}^-$ , leading to the decrease of pH (Eqs. (3) and (8)).

#### 4. Conclusions

The present study employed Fe/FeS magnetic nanoparticles as a novel and effective sorbent for Cr(VI) removal in batch and fixed-bed column experiments. The coating of FeS on the surface of  $\text{Fe}^0$  effectively prevented the aggregation of the particles, resulting in larger BET surface area and higher Cr(VI) removal efficiency than pure  $\text{Fe}^0$ . The removal of Cr(VI) by Fe/FeS mainly involved adsorption, reduction of Cr(VI) to Cr(III), and subsequent immobilization in the solid phase of  $(\text{Cr}_x\text{Fe}_{1-x})(\text{OH})_3$  and  $\text{FeCr}_2\text{S}_4$ . Moreover, the coating of FeS retarded the dissolution of Fe and thus reduced the toxicity of the particles. The findings in this work indicate that Fe/FeS nanoparticles hold the promise to be employed as an effective sorbent for immobilization of Cr(VI) in contaminated water and soil.

#### Acknowledgements

This work was supported by Tianjin Research Program of Application Foundation and Advanced Technology (15JCYBJC53800), National Natural Science Foundation of China (41503085, 31270544), Scientific Research Foundation for Returned Overseas Chinese Scholars, Ministry of Education of China ([2015]1098), and 863 achievement transformation program in Tianjin (No. 14RCHZSF00144).

#### Appendix A. Supplementary data

Supplementary data to this article can be found online at <http://dx.doi.org/10.1016/j.scitotenv.2017.03.282>.

#### References

- Alidokht, L., Khataee, A.R., Reyhanitabar, A., Oustan, S., 2011. Reductive removal of Cr(VI) by starch-stabilized  $\text{Fe}^0$  nanoparticles in aqueous solution. *Desalination* 270, 105–110.
- Alowitz, M.J., Scherer, M.M., 2002. Kinetics of nitrate, nitrite, and Cr(VI) reduction by iron metal. *Environ. Sci. Technol.* 36, 299–306.
- Altundogan, H.S., 2005. Cr(VI) removal from aqueous solution by iron (III) hydroxide-loaded sugar beet pulp. *Process Biochem.* 40, 1443–1452.
- Biesinger, M.C., Payne, B.P., Grosvenor, A.P., Lau, L.W.M., Gerson, A.R., Smart, R.S.C., 2011. Resolving surface chemical states in XPS analysis of first row transition metals, oxides and hydroxides: Cr, Mn, Fe, Co and Ni. *Appl. Surf. Sci.* 257, 2717–2730.
- Castro, V.D., Ciampi, S., 1995. XPS study of the growth and reactivity of Fe/MnO thin films. *Surf. Sci.* 331–333, 294–299.
- Çengelöglü, Y., Tor, A., Kir, E., Ersöz, M., 2003. Transport of hexavalent chromium through anion-exchange membranes. *Desalination* 154, 239–246.
- Crane, R.A., Scott, T.B., 2012. Nanoscale zero-valent iron: future prospects for an emerging water treatment technology. *J. Hazard. Mater.* 211–212, 112–125.
- Demoisson, F., Mullet, M., Humbert, B., 2005. Pyrite oxidation by hexavalent chromium: investigation of the chemical processes by monitoring of aqueous metal species. *Environ. Sci. Technol.* 39, 8747–8752.
- Donato, P.D., Mustin, C., Benoit, R., Erre, R., 1993. Spatial distribution of iron and sulphur species on the surface of pyrite. *Appl. Surf. Sci.* 68, 81–93.
- Fairley, N., 2016. [http://www.casaxps.com/help\\_manual/line\\_shapes.htm](http://www.casaxps.com/help_manual/line_shapes.htm) (© Casa Software Ltd.).
- Fu, F., Dionysiou, D.D., Liu, H., 2014. The use of zero-valent iron for groundwater remediation and wastewater treatment: a review. *J. Hazard. Mater.* 267, 194–205.
- Fu, R., Yang, Y., Xu, Z., Zhang, X., Guo, X., Bi, D., 2015. The removal of chromium (VI) and lead (II) from groundwater using sepiolite-supported nanoscale zero-valent iron (S-NZVI). *Chemosphere* 138, 726–734.
- Giasuddin, A.B.M., Kanel, S.R., Choi, H., 2007. Adsorption of humic acid onto nanoscale zerovalent iron and its effect on arsenic removal. *Environ. Sci. Technol.* 41, 2022–2027.
- Gong, Y., Liu, Y., Xiong, Z., Zhao, D., 2014. Immobilization of mercury by carboxymethyl cellulose stabilized iron sulfide nanoparticles: reaction mechanisms and effects of stabilizer and water chemistry. *Environ. Sci. Technol.* 48, 3986–3994.
- Gong, Y., Tang, J., Zhao, D., 2016. Application of iron sulfide particles for groundwater and soil remediation: a review. *Water Res.* 89, 309–320.
- Gupta, V.K., Agarwal, S., Saleh, T.A., 2011. Chromium removal by combining the magnetic properties of iron oxide with adsorption properties of carbon nanotubes. *Water Res.* 45, 2207–2212.
- Inyang, M., Gao, B., Zimmerman, A., Zhang, M., Chen, H., 2014. Synthesis, characterization, and dye sorption ability of carbon nanotube–biochar nanocomposites. *Chem. Eng. J.* 236, 39–46.
- Johnson, P.R., Sun, N., Elimelech, M., 1996. Colloid transport in geochemically heterogeneous porous media: modeling and measurements. *Environ. Sci. Technol.* 30, 3284–3293.
- Kantar, C., Ari, C., Keskin, S., Dogaroglu, Z.G., Karadeniz, A., Alten, A., 2015. Cr(VI) removal from aqueous systems using pyrite as the reducing agent: batch, spectroscopic and column experiments. *J. Contam. Hydrol.* 174, 28–38.
- Keller, A.A., Garner, K., Miller, R.J., Lenihan, H.S., 2012. Toxicity of nano-zero valent iron to freshwater and marine organisms. *PLoS One* 7, e43983.
- Kim, E.J., Kim, J.H., Azad, A.M., Chang, Y.S., 2011. Facile synthesis and characterization of Fe/FeS nanoparticles for environmental applications. *ACS Appl. Mater. Interfaces* 3, 1457–1462.
- Lan, Y., Deng, B., Kim, C., Thornton, D.C., Xu, H., 2005. Catalysis of elemental sulfur nanoparticles on chromium(VI) reduction by sulfide under anaerobic conditions. *Environ. Sci. Technol.* 39, 2087–2094.
- Lee, G., Park, J., Harvey, O.R., 2013. Reduction of chromium(VI) mediated by zero-valent magnesium under neutral pH conditions. *Water Res.* 47, 1136–1146.
- Li, Y., Jin, Z., Li, T., Xiu, Z., 2012. One-step synthesis and characterization of core-shell  $\text{Fe}@\text{SiO}_2$  nanocomposite for Cr(VI) reduction. *Sci. Total Environ.* 421–422, 260–266.
- Li, X., Ai, L., Jiang, J., 2016. Nanoscale zerovalent iron decorated on graphene nanosheets for Cr(VI) removal from aqueous solution: surface corrosion retard induced the enhanced performance. *Chem. Eng. J.* 288, 789–797.
- Manning, B.A., Kiser, J.R., Kwon, H., Kanel, S.R., 2007. Spectroscopic investigation of Cr(III)- and Cr(VI)-treated nanoscale zerovalent iron. *Environ. Sci. Technol.* 41, 586–592.
- Martin, J.E., Herzing, A.A., Yan, W., Li, X., Koel, B.E., Kiely, C.J., Zhang, W., 2008. Determination of the oxide layer thickness in core-shell zerovalent iron nanoparticles. *Langmuir* 24, 4329–4334.
- Melitas, N., Chuffe-Moscoco, O., Farrell, J., 2001. Kinetics of soluble chromium removal from contaminated water by zerovalent iron media: corrosion inhibition and passive oxide effects. *Environ. Sci. Technol.* 35, 3948–3953.
- Mullet, M., Boursiquot, S., Ehrhardt, J.J., 2004. Removal of hexavalent chromium from solutions by mackinawite, tetragonal FeS. *Colloids Surf. A Physicochem. Eng. Asp.* 244, 77–85.
- Mullet, M., Demoisson, F., Humbert, B., Michot, L.J., Vantelon, D., 2007. Aqueous Cr(VI) reduction by pyrite: speciation and characterisation of the solid phases by X-ray photoelectron, Raman and X-ray absorption spectroscopies. *Geochim. Cosmochim. Acta* 71, 3257–3271.
- Mullet, M., Khare, V., Ruby, C., 2008. XPS study of Fe(II)-Fe(III) (oxy)hydroxycarbonate green rust compounds. *Surf. Interface Anal.* 40, 323–328.
- Neal, A.L., Techkarnjanaruk, S., Dohnalkova, A., McCreedy, D., Peyton, B.M., Geesey, G.G., 2001. Iron sulfides and sulfur species produced at hematite surfaces in the presence of sulfate-reducing bacteria. *Geochim. Cosmochim. Acta* 65, 223–235.
- Nesbitt, H.W., Muir, I.J., 1994. X-ray photoelectron spectroscopic study of a pristine pyrite surface reacted with water vapour and air. *Geochim. Cosmochim. Acta* 58, 4667–4679.
- Patterson, R.R., Fendorf, S., 1997. Reduction of hexavalent chromium by amorphous iron sulfide. *Environ. Sci. Technol.* 31, 2039–2044.
- Pearson, G.R., 1988. Absolute electronegativity and hardness: application to inorganic chemistry. *Inorg. Chem.* 27, 734–740.
- Ponder, S.M., Darab, J.G., Mallouk, T.E., 2000. Remediation of Cr(VI) and Pb(II) aqueous solutions using supported, Nanoscale zero-valent iron. *Environ. Sci. Technol.* 34, 2564–2569.
- Powell, R.M., Puls, R.W., Hightower, S.K., Sabatini, D.A., 1995. Coupled iron corrosion and chromate reduction: mechanisms for subsurface remediation. *Environ. Sci. Technol.* 29, 1913–1922.
- Pratt, A.R., Nesbitt, H.W., Muir, I.J., 1994. Generation of acids from mine waste: oxidative leaching of pyrrhotite in dilute  $\text{H}_2\text{SO}_4$  solutions at pH 3.0. *Geochim. Cosmochim. Acta* 58, 5147–5159.
- Saleh, N., Kim, H.-J., Phenrat, T., Matyjaszewski, K., Tilton, R.D., Lowry, G.V., 2008. Ionic strength and composition affect the mobility of surface-modified  $\text{Fe}^0$  nanoparticles in water-saturated sand columns. *Environ. Sci. Technol.* 42, 3349–3355.
- Sarin, V., Singh, T.S., Pant, K.K., 2006. Thermodynamic and breakthrough column studies for the selective sorption of chromium from industrial effluent on activated eucalyptus bark. *Bioresour. Technol.* 97, 1986–1993.
- Sarkar, B., Xi, Y., Megharaj, M., Krishnamurti, G.S.R., Rajarathnam, D., Naidu, R., 2010. Remediation of hexavalent chromium through adsorption by bentonite based Arquad(R) 2HT-75 organoclays. *J. Hazard. Mater.* 183, 87–97.
- Schlautman, M.A., Han, I., 2001. Effects of pH and dissolved oxygen on the reduction of hexavalent chromium by dissolved ferrous iron in poorly buffered aqueous systems. *Water Res.* 35, 1534–1546.
- Shi, L., Zhang, X., Chen, Z., 2011. Removal of chromium (VI) from wastewater using bentonite-supported nanoscale zero-valent iron. *Water Res.* 45, 886–892.
- Stypula, B., Stoch, J., 1994. The characterization of passive films on chromium electrodes by XPS. *Corros. Sci.* 36, 2159–2167.
- Su, Y., Adeleye, A.S., Keller, A.A., Huang, Y., Dai, C., Zhou, X., Zhang, Y., 2015. Magnetic sulfide-modified nanoscale zerovalent iron (S-nZVI) for dissolved metal ion removal. *Water Res.* 74, 47–57.
- Tang, J., Huang, Y., Gong, Y., Lyu, H., Wang, Q., Ma, J., 2016. Preparation of a novel graphene oxide/Fe–Mn composite and its application for aqueous Hg(II) removal. *J. Hazard. Mater.* 316, 151–158.

- Thomas, J., Jones, C., Skinner, W., Smart, R., 1998. The role of surface sulfur species in the inhibition of pyrrhotite dissolution in acid conditions. *Geochim. Cosmochim. Acta* 62, 1555–1565.
- Vainshtein, M., Kusch, P., Mattusch, J., Vatsourina, A., Wiessner, A., 2003. Model experiments on the microbial removal of chromium from contaminated groundwater. *Water Res.* 37, 1401–1405.
- Villacis-García, M., Villalobos, M., Gutierrez-Ruiz, M., 2015. Optimizing the use of natural and synthetic magnetites with very small amounts of coarse Fe(0) particles for reduction of aqueous Cr(VI). *J. Hazard. Mater.* 281, 77–86.
- Wang, H., Yuan, X., Wu, Y., Chen, X., Leng, L., Wang, H., Li, H., Zeng, G., 2015a. Facile synthesis of polypyrrole decorated reduced graphene oxide–Fe<sub>3</sub>O<sub>4</sub> magnetic composites and its application for the Cr(VI) removal. *Chem. Eng. J.* 262, 597–606.
- Wang, H., Yuan, X., Wu, Y., Chen, X., Leng, L., Zeng, G., 2015b. Photodeposition of metal sulfides on titanium metal-organic frameworks for excellent visible-light-driven photocatalytic Cr(VI) reduction. *RSC Adv.* 5, 32531.
- Wang, H., Yuan, X., Wu, Y., Zeng, G., Chen, X., Leng, L., Wu, Z., Jiang, L., Li, H., 2015c. Facile synthesis of amino-functionalized titanium metal-organic frameworks and their superior visible-light photocatalytic activity for Cr(VI) reduction. *J. Hazard. Mater.* 286, 187–194.
- Wang, T., Bian, X., Yang, C., Zhao, S., Yu, M., 2017. Ferrofluids based on Co-Fe-Si-B amorphous nanoparticles. *Appl. Surf. Sci.* 399, 663–669.
- Wharton, M.J., Atkins, B., Charnock, J.M., Livens, F.R., Patrick, R.A.D., Collison, D., 2000. An X-ray absorption spectroscopy study of the coprecipitation of Tc and Re with mackinawite (FeS). *Appl. Geochem.* 15, 347–354.
- Wilkin, R.T., Su, C., Ford, R.G., Paul, C.J., 2005. Chromium removal processes during groundwater remediation by a zerovalent iron permeable reactive barrier. *Environ. Sci. Technol.* 39, 4599–4605.
- Wolthers, M., Charlet, L., van Der Linde, P.R., Rickard, D., van Der Weijden, C.H., 2005. Surface chemistry of disordered mackinawite (FeS). *Geochim. Cosmochim. Acta* 69, 3469–3481.
- Xiu, Z., Gregory, K.B., Lowry, G.V., Alvarez, P.J.J., 2010. Effect of bare and coated nanoscale zerovalent iron on tceA and vcrA gene expression in *dehalococcoides* spp. *Environ. Sci. Technol.* 44, 7647–7651.
- Xu, Y., Schoonen, M.A.A., 2000. The absolute energy positions of conduction and valence bands of selected semiconducting minerals. *Am. Mineral.* 85, 543–556.
- Yamashita, T., Hayes, P., 2008. Analysis of XPS spectra of Fe<sup>2+</sup> and Fe<sup>3+</sup> ions in oxide materials. *Appl. Surf. Sci.* 254, 2441–2449.
- Yang, R., Wang, Y., Li, M., Hong, Y., 2014. A new carbon/ferrous sulfide/iron composite prepared by an in situ carbonization reduction method from hemp (*Cannabis sativa* L.) stems and its Cr(VI) removal ability. *ACS Sustain. Chem. Eng.* 2, 1270–1279.
- Yoon, I.H., Bang, S., Chang, J.S., Gyu Kim, M., Kim, K.W., 2011. Effects of pH and dissolved oxygen on Cr(VI) removal in Fe(0)/H<sub>2</sub>O systems. *J. Hazard. Mater.* 186, 855–862.
- Zhang, Y., Su, Y., Zhou, X., Dai, C., Keller, A.A., 2013. A new insight on the core-shell structure of zerovalent iron nanoparticles and its application for Pb(II) sequestration. *J. Hazard. Mater.* 263, 685–693.